ADVANCES IN ATMOSPHERIC SCIENCES, VOL. 26, NO. 6, 2009, 1241–1252

Numerical Study of Flow and Gas Diffusion in the Near-Wake behind an Isolated Building

Mohamed F. YASSIN*[1,2]

[1] *Department of Environmental Technology Management, College for Women, Kuwait University, P.O. Box* 5969*, Kuwait, Safat* 13060*, Kuwait*

[2] *Faculty of Engineering, Assiut University, Assiut*-71516*, Egypt*

(Received 27 February 2008; revised 11 January 2009)

ABSTRACT

To assist validation of the experimental data of urban pollution dispersion, the effect of an isolated building on the flow and gaseous diffusion in the wake region have been investigated numerically in the neutrally stratified rough-walled turbulent boundary layer. Numerical studies were carried out using Computational Fluid Dynamics (CFD) models. The CFD models used for the simulation were based on the steady-state Reynolds-Average Navier-Stoke equations (RANS) with κ-ε turbulence models; standard κ-ε and RNG κ-ε models. Inlet conditions and boundary conditions were specified numerically to the best information available for each fluid modeling simulation. A gas pollutant was emitted from a point source within the recirculation cavity behind the building model. The accuracy of these simulations was examined by comparing the predicted results with wind tunnel experimental data. It was confirmed that simulation using the model accurately reproduces the velocity and concentration diffusion fields with a fine-mish resolution in the near wake region. Results indicated that there is a good agreement between the numerical simulation and the wind tunnel experiment for both wind flow and concentration diffusion. The results of this work can help to improve the understanding of mechanisms of and simulation of pollutant transport in an urban environment.

Key words: atmospheric turbulence, CFD model, isolated building, pollutant dispersion

Citation: Yassin, M. F., 2009: Numerical study of flow and gas diffusion in the near-wake behind an isolated building. *Adv. Atmos. Sci.*, **26**(6), 1241–1252, doi: 10.1007/s00376-009-8025-7.

1. Introduction

The flow and dispersion of atmospheric pollutants in the near-wake region downwind of buildings is a complex problem. However, the prediction of likely concentration levels in any particular situation is often an important requirement for which there are at present no universally applicable rules. Therefore, investigations on the distribution of pollutants in the near-wake region of buildings are necessary to understand more clearly the complicated dispersion processes caused by disturbed air motions near buildings. The aerodynamics of wake flow, and thus pollution concentration, are highly dependent on building shape, length scale, and the boundary layer.

The distribution of pollution in the near-wake region of a high-rise building is strongly influenced by both the scales of the boundary layer and vortex shedding. Lateral and vertical mixing initially spread the pollution over the width and the height of the building, respectively. The pollution concentration is also influenced by the downstream extent and residence time of recirculating flow (Hinds, 1969; Fackrell, 1984; Hunt and Castro, 1984). Downstream of recirculation mixing, mean concentrations are inversely related to the cross-stream area of the wake flow. For a continuous source of pollution in the near-wake region, the spatial distribution of average concentration represents the superposition of a series of instantaneous distributions, characterizing the mixing process. The variation within the series reflects the transient nature of building-induced vortex shedding and the interaction of the building wake flow with the boundary layer flow. In the field, variation in the wind direction, wind

*Corresponding author: Mohamed F. YASSIN, Mohamed_f_yassin@hotmail.com

speed, and atmospheric stability can also significantly influence the overall distribution of pollution concentration.

Several studies have been conducted to understand the flow structure and dispersion characteristics behind a simple building in a laboratory using wind tunnel experiments and numerical models, e.g., Halitsky (1963); Robins and Castro (1977); Hunt et al. (1978); Li and Meroney (1983a,b); Hosker (1984); Huber (1989); Isaacson and Sandri (1990); Higson et al. (1994); Snyder (1994); Saathoff et al. (1995); Macdonald et al. (1998); Flowe and Kumar (2000); Mavroidis and Griffiths (2001); Sada and Sato (2002); Mfula et al. (2005). These studies tended to focus on either the turbulence structures or pollutant distributions/fluctuations in the building wake under a fixed release condition due to resource or computational constraints. Generalization of the findings of these studies would not be representative for releases within the cavity region. Only few simulation studies of air pollution dispersion appear to have been carried out (Dawson et al., 1991; Zhang et al., 1992). In these works, the flow field around buildings has been sufficiently estimated with transport characteristics (convection, diffusion) so that the scalar pollutant distribution could be derived from it. Such transport characteristics would be appropriate for passive scalar transport. Li and Stathopoulos (1997, 1998) attempted to evaluate the air pollution distribution around a building by solving the concentration equation based on the previously simulated wind field. They presented the numerical simulation of air pollutant dispersion around cubic and rectangular buildings by using the standard κ-ε turbulence model. Olvera et al. (2008) performed the dispersion simulations of buoyant and natural plume release within the recirculation cavity behind a cubical building using a commercially available CFD code and the RNG κ-ε turbulence model. They illustrated the complex effects of plume buoyancy on the flow structure and concentration distribution in the near-wake region.

This paper presents the results of numerical simulations investigating the effect of isolated obstacle on the flow and pollutant dispersion in the boundary layer in an urban environment using CFD models under neutral conditions at various locations in the downwind region. Thus, the aim of the present work is to improve the understanding of mechanisms impacting the flow and pollutant dispersion effects related to obstacles in an urban environment, also utilizing and validating the corresponding wind tunnel data. A three-dimensional model based on Reynolds-Average Navier-Stoke equations (RANS) coupled with κ-ε turbulence models; the standard κ-ε model, and a RNG κ-ε turbulence closure model were used for the simulations. In addition, a transport equation for the passive scalar was solved to simulate pollutant dispersion.

2. Numerical methodology

In this paper, the numerical simulations were performed using the commercial CFD code FLUENT (Fluent, 2005), which is based on the finite volume method to solve the equations of conservation for the different transported quantities in the flow (mass, momentum, energy, concentration). The code first performs the coupled resolution of the pressure and velocity fields and then evolution of other parameters, like gas concentration.

2.1 *Modeling domain*

The geometrical model for the atmospheric boundary layer flow in the near wake region of the high-rise building is shown in Fig. 1. The geometry is identical to that examined experimentally in a wind tunnel by Yassin et al. (2008) where a rectangular building model of equivalent height H, $0.5H$ length, and $0.5H$ width is placed in a simulated atmospheric boundary layer of height $= 3H$, where H is the building height $=$ 0.2 m and the profile reach 0.6 m in Fig. 2. The high-rise building is modeled on a 1:500 scale. The building model was placed on a ground plane as shown in Fig. 1 and this configuration represented typical environmental conditions for the building model.

A three-dimensional modeling domain of $43H$ in the longitudinal direction, $17.5H$ in the lateral direction, and $12.5H$ in the vertical direction was defined. A 0.2 m high building mounted on the bottom surface was centered at $17.5H$ from the inlet face. Although the domain is slightly smaller than suggested standards (Franke, 2006), no velocity gradients at the

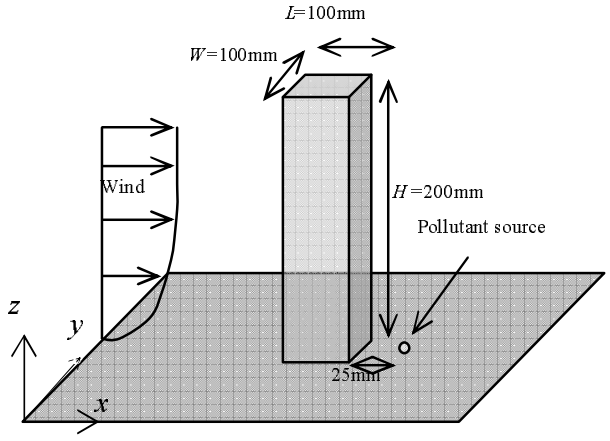

Fig. 1. Geometry of high-rise building.

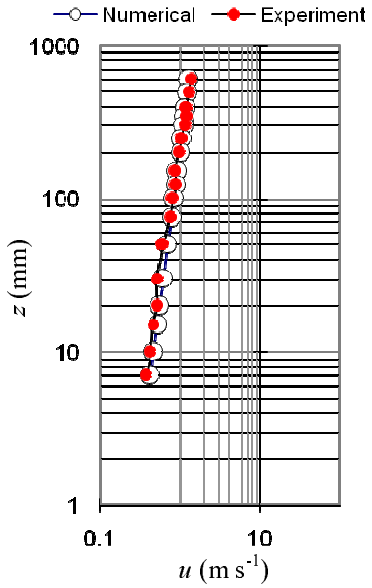

Fig. 2. Inlet atmospheric boundary layer profile.

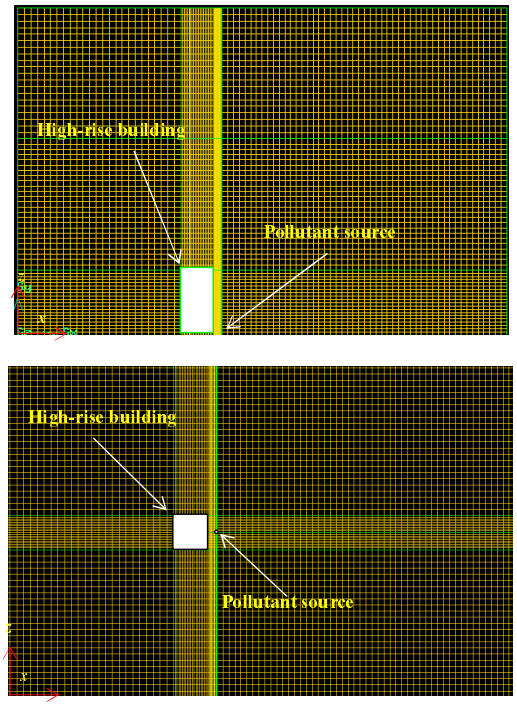

Fig. 3. Computational domain and mesh division.

boundaries were observed and optimal computational requirements were achieved. The origin of the domain was defined at the center of the lower edge of the building's lee wall. Gas pollutant was emitted from the point source with a diameter of $0.02H$, located at $0.125H$ in the building model. No-slip conditions were defined at the solid surface. An outflow boundary was defined opposite to the inlet boundary.

The domain of interest was generated and then meshed using the integrated preprocessor of FLUENT and GAMBIT packages. Fine cells were defined near the building, where high gradients were expected, and coarse cells elsewhere. Additionally, six high-resolution mesh layers were generated near solid boundaries. A mesh refinement test was performed to identify the optimal mesh resolution and ensure the results were mesh-independent. Flow over an isolated building under neutral atmospheric conditions was simulated during the refinement test. The computational mesh employed was a conventional nonuniform mesh, for which the optimal mesh was identified, consisting of 650 000 cells of average side sizes. A typical grid configuration in the recirculation cavity of the building model is shown in Fig. 3. To minimize truncation error, cell-size increments were gradual and limited to a maximum increment of 25% between contiguous cells.

2.2 *Governing equations*

The fluid flow was modeled by partial differential equations describing the conservation of mass, momentum, and species concentration in three rectangular Cartesian coordinate directions, solving for steady, incompressible flow, which after Reynolds averaging becomes:

The continuity equation is given by

$$\frac{\partial u_i}{\partial x_i} = 0 \tag{1}$$

where u_i is the ith mean component.

The momentum equation given by

$$\frac{\partial u_i}{\partial t} + \frac{\partial}{\partial x_j}(u_j u_i) = -\frac{1}{\rho}\frac{\partial p}{\partial x_i} + \frac{\partial}{\partial x_j}\left\{\nu\left(\frac{\partial u_i}{\partial x_j} + \frac{\partial u_j}{\partial x_i}\right) - \overline{u_i' u_j'}\right\} \tag{2}$$

where p is the deviation of pressure from its reference value, ρ is the air density, and ν is the kinematic viscosity of air.

The species transport equation is given by

$$\frac{\partial c}{\partial t} + \frac{\partial u_j c}{\partial x_j} = \frac{\partial}{\partial x_j}\left(D\frac{\partial c}{\partial x_j} - \overline{c' u_j'}\right) + S_c \tag{3}$$

where c is the mean concentration of any passive scalar (say, any pollutant), u' and c' are fluctuations from their u_i and c mean values, respectively, D is the molecular diffusivity of the pollutant, and S_c denotes the source of pollutant.

The Reynolds stress and turbulent flux in Eqs. (2) and (3) are parameterized in terms of grid-resolvable

variables as:

$$-\overline{u_i' u_j'} = \nu_t \left(\frac{\partial u_i}{\partial x_j} + \frac{\partial u_j}{\partial u_i} \right) - \frac{2}{3} T_{\mathrm{KE}} \delta_{ij} \tag{4}$$

$$-\overline{c' u_j'} = \nu_c \frac{\partial c}{\partial x_j} \tag{5}$$

$$\nu_t = c_\mu \frac{T_{\mathrm{KE}}^2}{\varepsilon} \tag{6}$$

$$S_{c_t} = \frac{v_t}{v_c} \tag{7}$$

where ν_t and ν_c are the turbulent viscosities of momentum and pollutant concentration, respectively, and δ_{ij} is the kronecker delta. T_{KE} and ε stand for the turbulence kinetic energy and its rate of dissipation. The value of $c_\mu = 0.09$.

The turbulent energy transport equation is given by:

$$\frac{\partial T_{\mathrm{KE}}}{\partial t} + \frac{\partial T_{\mathrm{KE}} u_i}{\partial x_i} = \frac{\partial}{\partial x_i} \left(\frac{\nu_t}{\sigma_k} \frac{\partial T_{\mathrm{KE}}}{\partial x_i} \right) + \nu_t \left(\frac{\partial u_i}{\partial x_j} + \frac{\partial u_j}{\partial x_i} \right) \frac{\partial u_i}{\partial x_j} - \varepsilon \,. \tag{8}$$

To model the turbulent dissipation rate, the standard κ-ε model (Launder and Spalding, 1974) and RNG κ-ε model (Yakhot et al., 1992) are adopted here for computational efficiency and accuracy. The RNG κ-ε model differs from the standard κ-ε turbulence scheme only through the modification to the equation for ε, which includes an additional sink term in the turbulence dissipation equation to account for non-equilibrium strain rates and employs different values for the model coefficients (Kim and Baik, 2004). The turbulent dissipation rate in the standard κ-ε model is expressed by the following equation:

$$\frac{\partial \varepsilon}{\partial t} + \frac{\partial \varepsilon u_i}{\partial x_i} = \frac{\partial}{\partial x_i} \left(\frac{\nu_t}{\sigma_\varepsilon} \frac{\partial \varepsilon}{\partial x_i} \right) + c_{1\varepsilon} \frac{\varepsilon}{T_{\mathrm{KE}}} \nu_t \left(\frac{\partial u_i}{\partial x_j} + \frac{\partial u_j}{\partial x_i} \right) \frac{\partial u_i}{\partial x_j} - c_{2\varepsilon} \frac{\varepsilon^2}{T_{\mathrm{KE}}} \,. \tag{9}$$

On other hand, the turbulent dissipation rate in the RNG κ-ε model expressed by the following equation:

$$\frac{\partial \varepsilon}{\partial t} + \frac{\partial \varepsilon u_i}{\partial x_i} = \frac{\partial}{\partial x_i} \left(\frac{\nu_t}{\sigma_\varepsilon} \frac{\partial \varepsilon}{\partial x_i} \right) + c_{ls} \frac{\varepsilon}{T_{\mathrm{KE}}} \nu_t \left(\frac{\partial u_i}{\partial x_j} + \frac{\partial u_j}{\partial x_i} \right) \frac{\partial u_i}{\partial x_j} - c_{2\varepsilon} \frac{\varepsilon^2}{T_{\mathrm{KE}}} - R \,. \tag{10}$$

where $\sigma_k = 1.0$, $\sigma_\varepsilon = 1.3$, $c_{1\varepsilon} = 1.44$, $c_{2\varepsilon} = 1.92$, $Sc_t = 0.9$. The last term on right-hand side of Eq. (10) is an extra strain rate given by

$$R = c_\mu \eta^3 \varepsilon^2 \frac{1 - \eta/\eta_0}{k(1 + \beta_0 \eta^3)} \tag{11}$$

with

$$\eta = \frac{T_{\mathrm{KE}}}{\varepsilon} \left\{ \left(\frac{\partial u_i}{\partial x_j} + \frac{\partial u_j}{\partial x_i} \right) \frac{\partial u_i}{\partial x_j} \right\}^{1/2} . \tag{12}$$

where $\eta = 4.38$ and $\beta_0 = 0.012$.

In modeling urban flow and dispersion, smaller grid sizes are desirable in a building model to better resolve flow and dispersion field. To make the CFD model efficient for a given computing resource, a non-uniform grid system is implemented in the model. The above governing equations are solved numerically on a staggered grid system using a finite-volume method with the semi-implicit method using a pressure-linked equation (SIMPLE) algorithm (Patanker, 1980). The numerical procedure is detailed in Baik et al. (2003).

2.3 *Boundary conditions*

A wall function was employed in the near-wake region. The inlet velocity profile for the atmospheric boundary layer was applied based on the wind profile from the experimental data of Yassin et al. (2008), as shown in Fig. 2. The effect of surface roughness on the flow structure immediately behind the building is low because the cavity region is highly turbulent and a Reynolds number of 14053 was considered. The 1/4th power law is used to specify the x velocity components:

$$U \alpha Z^{0.25} \,. \tag{13}$$

The inlet profiles for the turbulence kinetic energy T_{KE} and dissipation rate ε are found in Fluent (2005):

$$T_{\mathrm{KE}} = \frac{u_\tau^2}{\sqrt{c_\mu}} \tag{14}$$

$$\varepsilon = \frac{c_\mu^{3/4} (T_{\mathrm{KE}}^{3/2})}{l} \tag{15}$$

where u_τ is the friction velocity and l is the turbulence length scale. For more details about Eqs. (13) and (14), refer to Fluent (2005).

3. Results and discussion

3.1 *Model validation*

The aim of the numerical simulation is to generate a reliable wind environment for the study of dispersion from the ground level source. The three-dimensional CFD model with the standard κ-ε turbulence model was compared with that of the RNG κ-ε turbulence model and validated against the wind tunnel data of Yassin et al. (2008). The simulated data were interpolated at the same grid points in the wind tunnel experiment. All concentrations were presented in a dimensionless form; they are presented here in terms of the ratio K

$$K = CU_H H^2/Q\,, \tag{16}$$

where C is the actual concentration, H is the height of the building model, U_H is the free-stream wind velocity at a height of the building model, and Q is the source strength. The comparison between experimental data and simulation results at different locations behind the building model are presented in Figs. 4, 6, 10, 12, and 13. The standard and RNG κ-ε turbulence model results were consistent reasonably well with the wind tunnel results.

3.2 *Flow field simulations*

The near-wake structure is characterized by a recirculation cavity region behind the building. The recirculation cavity is a region characterized by low mean velocity and high turbulence relative to the approaching wind flow (Peterka et al., 1985). The most intense movement of the flow appears in the recirculation cavity region downwind of the high-rise building. Thus, the flow becomes very complex in this region. A close inspection of the velocity field is necessary for qualitative comparison of turbulence models used for study calculations.

3.2.1 *Mean flow field*

The mean velocity components are normalized by the reference velocity U_H at the building height H in the boundary layer. The simulated profile of mean velocity compared with the experimental data in the near-wake region of the building at various points (x/H = 0.125, 0.375, and 0.625) are shown in Fig. 4. A rapid increment of the mean velocity with height in the recirculation cavity region was observed. Such rapid increments imply large velocity strain and active production of turbulent kinetic energy. The simulated velocities in the upper region above $z/H = 1.0$ were in agreement with wind tunnel data. However, the magnitudes of the velocity in the lower region were small compared with those in the upper layer. This is because the magnitude of the momentum transfer from the upper region into the lower region was smaller than that of the upper layer transport by the ambient wind. The simulated velocities using the κ-ε turbulence models were lower than those from the experimental data. Furthermore, there is very little difference between the results from the standard κ-ε model and these from the RNG κ-ε model in surface layer. The simulated velocities near the ground level using the RNG κ-ε model matched observations better than those using the standard κ-ε model, except at x/H = 0.125 and 0.625. The difference in the results was not surprising since this area is hardest to simulate using both the numerical simulations and in wind tunnel experiments. This can in turn be attributed to the incorrect assignment of boundary conditions in the computational model. Due to a lack of very detailed information, it is not

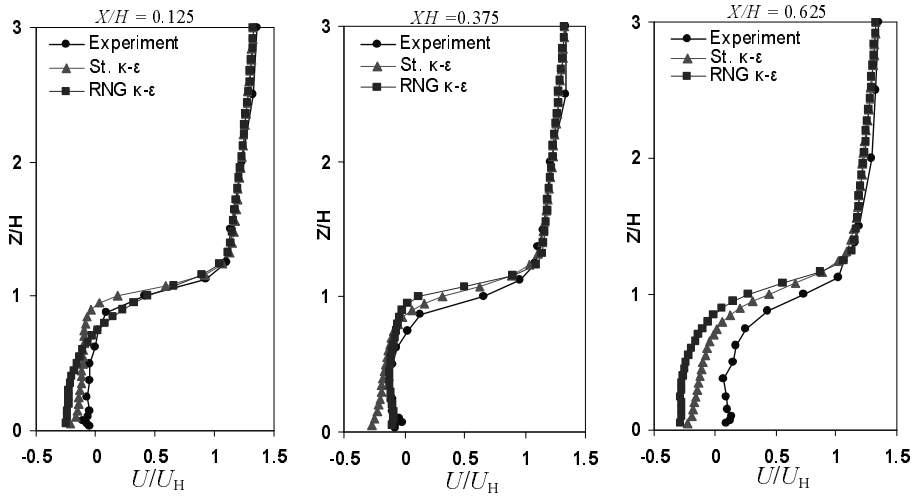

Fig. 4. Mean streamwise velocity, U/U_H.

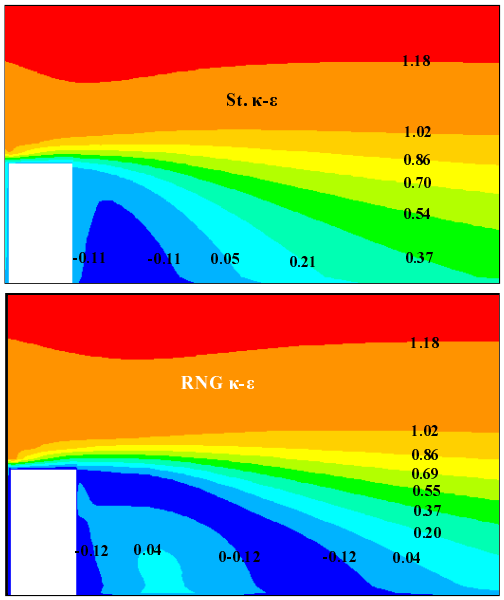

Fig. 5. Contour lines of the mean stream wise velocity in the x-z plane at $y/H = 0.0$: (top) standard k-ε turbulences and (bottom) RNG k-ε turbulences.

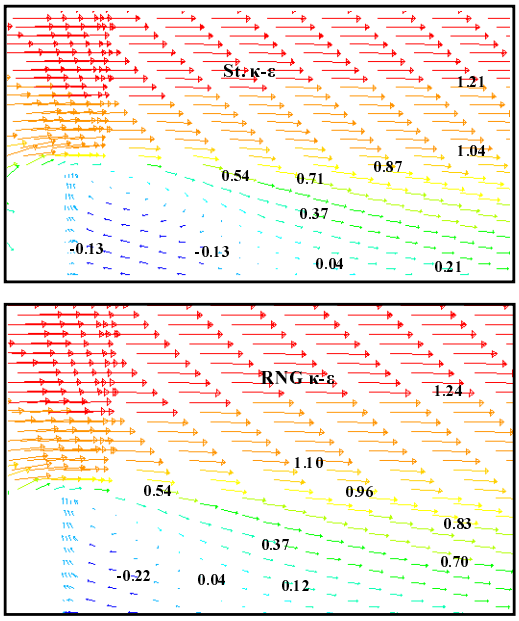

Fig. 6. Mean velocity vectors in the x-z plane at $y/H = 0.0$: (top) standard k-ε turbulences and (bottom) RNG k-ε turbulences.

possible to simulate precisely the boundary conditions of the wind tunnel. Near the top of the building, the simulated data was in poor agreement with the wind tunnel data, except the computed data for the RNG κ-ε model at $x/H = 0.125$, which was in good agreement with the experimental data. In general, there is a discrepancy between the data from the κ-ε turbulence models and experimental data near the top of the building, which may be mainly due to the simple upper boundary condition employed. In addition, the method for generating the simulated boundary layer generates a much deeper boundary layer in a limited downstream distance than a naturally developed boundary layer (Counihan, 1969). Therefore, it is very difficult to simulate the whole depth of this boundary layer accurately. Generally, the agreement between the numerically simulated results with the wind tunnel experiment data is quite encouraging in the near-wake region of the building. Figure 5 illustrates the contour lines of dimensionless mean velocity in the x-z plane at $y/H = 0.0$. The characteristics of the horizontal and vertical distributions of the mean velocity obtained by the RNG κ-ε model were similar to those obtained by the standard κ-ε model. However, a low value of the mean velocity was observed with the standard κ-ε turbulence model. The range of the recirculation cavity region of the building was observed to be narrow with the standard κ-ε turbulence model and expanded with the RNG κ-ε turbulence model.

Velocity filed vector diagrams in a plane were developed from the simulated flow at several locations. The x-z plane velocity vector field at $y/H = 0.0$ is shown in Fig. 6. There is no difference between the standard κ-ε and RNG κ-ε model. It was too small to allow for a detailed comparison in the vector plots. The x-z plane of the wind vector field was placed in cross-section of the portal vortex and the small vortex rotating anticlockwise near the top of the building. There is evidence that the top of the portal vortex is slightly tilted towards the upwind region. Flow attachments were observed more quickly from the RNG κ-ε model than those from the standard κ-ε model. The reattachmens in the simulated velocities are forming at the point nearest to the ground from the leeward face of the building. The reattachment distance with the RNG κ-ε model was longer than that with the standard κ-ε model. A reverse flow in the near wake region appeared; this is probably because the momentum transfer into the wake region is large. The momentum transfer can take place due to the different lengths of streamlines, along which momentum transfer from the ambient wind into the vortex occurs. Significant reverse flow exists in the recirculation cavity region, with only a relatively small region of forward-moving flow towards the top of the building, indicating that there must be significant three-dimensionality involved in the flow of the recirculation cavity region.

The x-y and x-z planes of the path lines for the mean velocity at $z/H = 0.5$ and $y/H = 0.0$ are shown

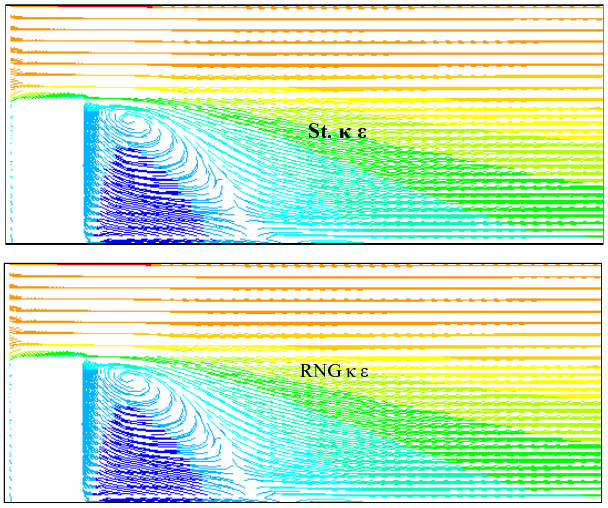

Fig. 7. Path lines for the mean velocity in the x-z and at $y/H = 0.0$: (top) standard k-ε turbulences and (bottom) RNG k-ε turbulences.

in Fig. 7. The path lines show the recirculation zone in the recirculation cavity region very clearly. A symmetric double-vortex circulation was found, but its intensity was weaker and not effective for the transportation of pollutant. The length of the recirculation zone behind the building can be seen in these figures. The length of the leeward recirculation was slightly less than $2H$, measured from the leeward face of the building. Beyond the double-vortex circulation, the flow was characterized by a relatively strong velocity. One of the effects of this is horizontal double-vortex circulation with the familiar horseshoe vortex pattern as described by (Oke, 1987). The horizontal double-vortex circulation and vertical vortices both require a counter-flow towards the lee wall of the upwind building- between the two vortexes and beneath the vortex. The velocity field obtained from the κ-ε turbulence models shows a vortex rotating in the upper part of the wake region. The rate of rotation of the vortex was the highest among all computational solution. In each vortex, the mean velocity was weaker near the upwind building region than in the downwind direction. Skimming flow was observed in both the standard κ-ε and RNG κ-ε models. The horizontal length recirculation zone in the RNG κ-ε model was larger than that in the standard κ-ε model. A small difference between the standard κ-ε and RNG κ-ε model can be found near the top height of a building, especially in a skimming flow. The main characteristics of skimming flow in both the standard κ-ε and RNK κ-ε models are that the vertical extent of the vortex is restricted below the roof-level of the high-rise building and the wind direction above the building is parallel to the roof-level.

3.2.2 *Turbulent flow field*

The simulated data compared with the experimental data for the normalized turbulence intensity in the recirculation cavity region are plotted in Fig. 8. The comparison of turbulence intensities was more complicated. The numerical results obtained from the standard κ-ε turbulence model were reported reasonably well near the top of the building compared with the experimental results. The difference between the numerical data from the RNG κ-ε model and the experimental data were larger in the near wake region than those from the standard κ-ε model. The peak value

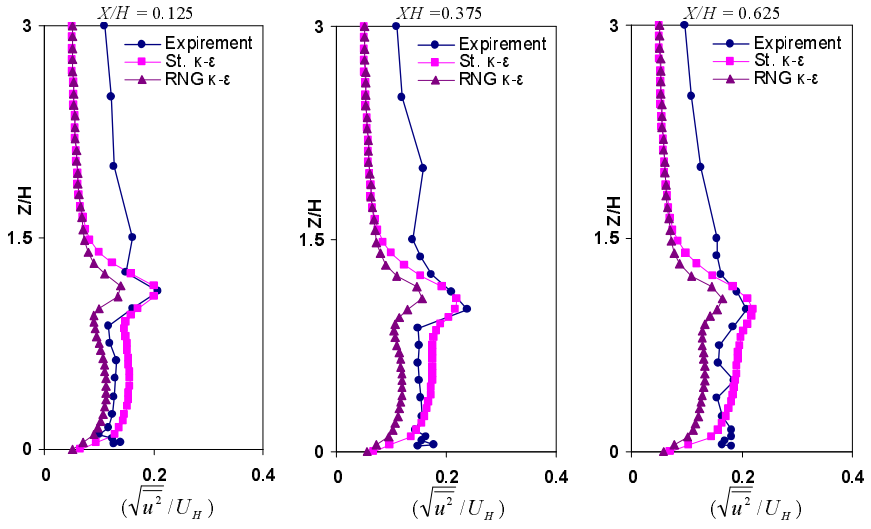

Fig. 8. Turbulent intensity in the downwind direction ($\sqrt{u^2}/U_H$).

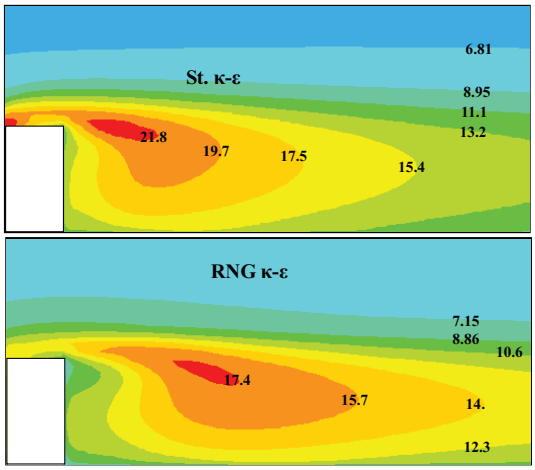

Fig. 9. Contour lines of the turbulent intensity in the x-z plane at $y/H = 0.0$: (top) standard k-ε turbulences and (bottom) RNG k-ε turbulences.

of the numerical data and the experimental data was found near the top of the building due to the large velocity gradient. In general, the numerical simulated results are quite reasonable compared with the wind tunnel experimental results. The contour lines of the turbulence intensity in the x-z plane at $y/H = 0.0$ and in the x-y plane at $z/H = 0.5$ are shown in Fig. 9. The simulated results from the standard κ-ε model were higher than that from the RNG κ-ε model. The horizontal and vertical distributions of the turbulence intensity were expanded in the wake region with the RNG κ-ε model and narrow with the standard κ-ε model.

A turbulent kinetic energy is one of the important quantities representing turbulence intensity. The turbulent kinetic energy is produced by buoyancy (if the thermodynamic energy equation is included) and wind shear and dissipated by viscosity in the turbulent flow. In order to maintain turbulence, the production of the turbulent kinetic energy must continue, and Fig. 10 shows the comparison of the numerically simulated vertical profile of the normalized turbulent kinetic energy with the wind tunnel experiment data. A high value of the turbulent kinetic energy was observed near the top of the building because of the existence of strong vertical shear of the streamwise velocity. This is mainly due to the increased turbulent kinetic energy production by mechanical wind shear at the top of the building. The maximum of the turbulent kinetic energy determined using the wind tunnel experiment was almost equal to that calculated using the standard κ-ε model, except at $x/H = 0.625$. The simulated results from the standard κ-ε model in the near-wake region were higher than that from the RNG κ-ε model. The simulated data from the standard κ-ε model in the near wake region were close with those from the wind tunnel data at $x/H = 0.125$ and 0.375 and differ at $x/H = 0.625$. The agreement between the numerically simulated and experimental results for height $1 < z/H < 3$ was observed to be large.

The contour lines of the turbulent kinetic energy are presented in Fig. 11. The simulated data from the standard κ-ε models exhibited characteristics similar to those from the RNG κ-ε model. The values of the turbulent kinetic energy from the RNG κ-ε model were observed to be less than that from the standard κ-ε

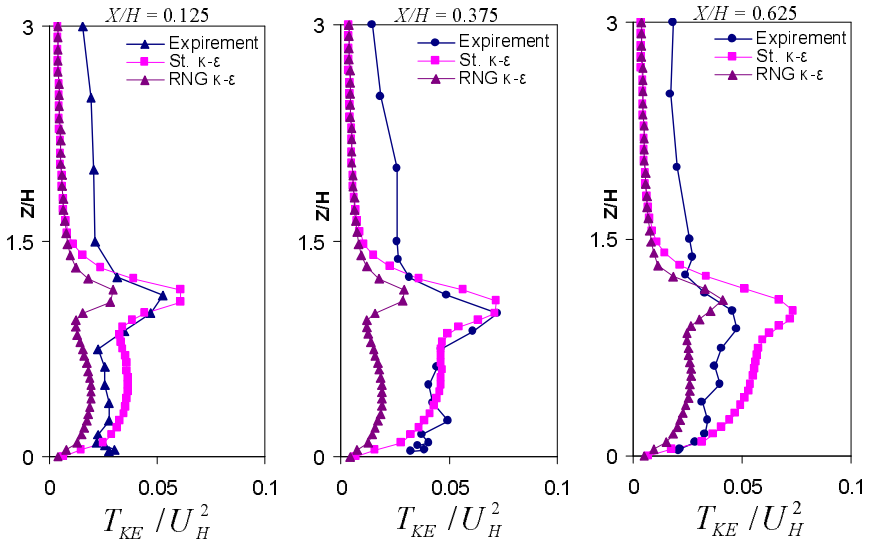

Fig. 10. Turbulent kinetic energy.

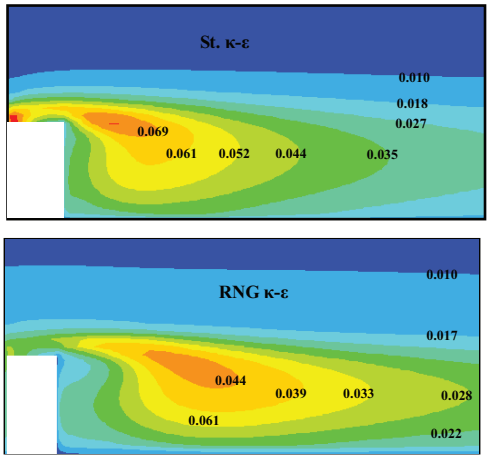

Fig. 11. Contour lines of turbulent kinetic energy in the x-z plane at $y/H = 0.0$: (top) standard k-ε turbulences and (bottom) RNG k-ε turbulences.

model. However, the horizontal and vertical distributions were expanded in the stream-wise direction with the RNG κ-ε model.

3.3 *Diffusion concentration simulations*

To investigate the dispersion characteristics in the recirculation cavity region downwind of the high-rise building, a pollutant source was emitted from the ground level at $x/H = 0.125$. The effluent velocity is 10% U_H. Figures 12 and 13 show the comparison of the present simulation results with the wind tunnel experiment results for the vertical and lateral profiles of the mean concentration at various locations in the recirculation cavity region: $x/H = 0.375$, 0.625, and 1.125.

The concentration results are lower than that of the experimental data, which is probably due to a reduced flux of concentration at top level of the building; otherwise, the agreement is very good. The concentration results using the RNG κ-ε model are lower than that using the standard κ-ε model. This is due to the lower turbulent kinetic energy, simulated in the RNG κ-ε model. The simulated results displayed the maximum concentration diffusion approximately at height $z/H = 0.2$ in the recirculation region and then decreasing similarly to the experimental data. The simulated results appeared to have maximum concentration near the ground level which is different from the experimental results. The simulated results predicted similar concentration diffusion with experimental results, except near the ground. The concentration results with the standard κ-ε model were observed to be in agreement with the experimental results. Although the pollutant source was released at $x/H = 0.125$, the centerline of the non-buoyancy plume was simulated to be at an elevated position of $z/H = 0.2$ in the near-wake region, because of rising flow over the building and its separation region. There was an increment in the diffusion concentration near the pollutant source at $x/H = 0.375$ and a narrow plume spread at the further leeward position in the near-wake region, at $x/H = 0.625$ and 1.125. According to this plume spread, maximum concentration values of the plume center at elevated positions decrease in the near wake region. The plume was calculated to be partially diffused into the wake region, and reaches its smallest value at $x/H = 1.125$.

A comparison of these features of simulated diffusion concentration with those obtained in the experimental results reveals some discrepancies. The maximum simulated concentration was slightly smaller

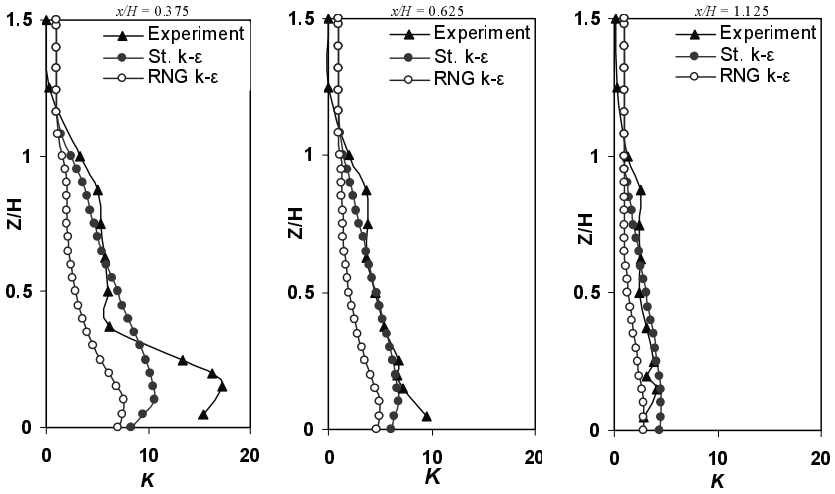

Fig. 12. Vertical profiles of non-dimensional mean concentration k.

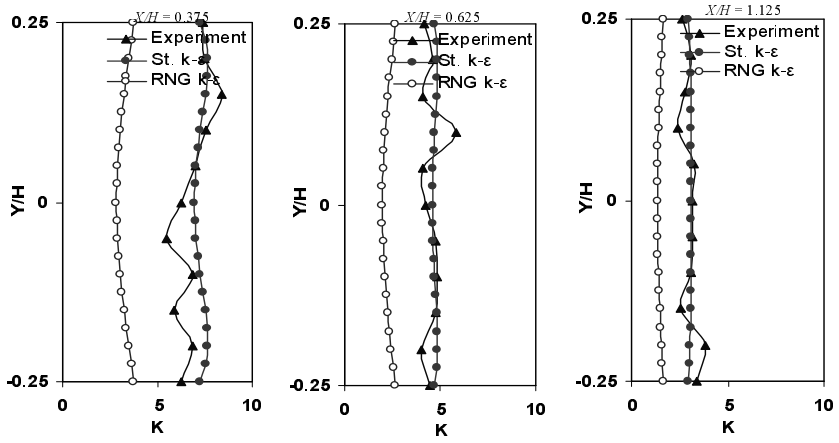

Fig. 13. Lateral profiles of non-dimensional mean concentration k.

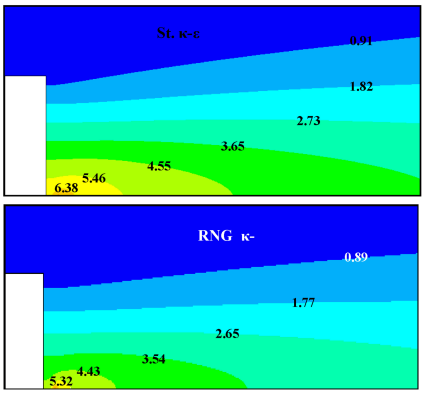

Fig. 14. Contour lines of non-dimensional mean concentration k in the x-z plane at $y/H = 0.0$: (top) standard k-ε turbulences and (bottom) RNG k-ε turbulences.

than that obtained in the wind tunnel experiment at $x/H = 0.375$ and 0.625. This is because of the rapid diffusion of the plume in the simulation caused by the slightly higher calculated turbulence intensity (Figs. 8 and 9). Although there are some discrepancies between the simulation results and those of the experimental results.

The contour of the concentration results at $z/H = 0.075$ (pedestrian level, $z = 1.5$ m) and $y/H = 0$ are shown in Figs. 14 and 15. Note that contour shapes were preserved, but the magnitudes differ. High levels of concentration diffusion occur downwind of the source, which gradually reduces as the plume moves up the back of the building. There is a region of low velocity and high turbulence from the upper area to the bottom of the wake region. The concentration diffusion was very high near the source location due to the increasing source buoyancy or momentum flux. The area of the minimum concentrations is shifted downwind of the source. The simulated patterns indicate that the area of maximum concentration is widespread, occupying the width of the building. The lateral spreading was facilitated by the streamwise flow in the recirculation cavity. Otherwise, concentration diffusion was observed small near the top of the building. Moreover, the lowest concentration in the recirculation cavity region appeared near the upwind area of building. This

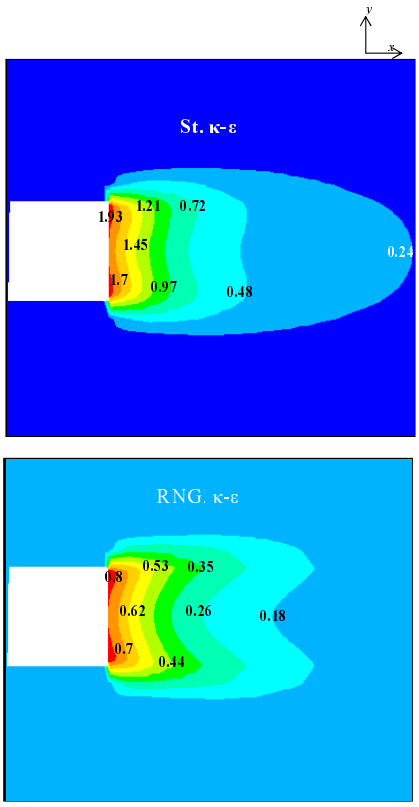

Fig. 15. Contour lines of non-dimensional mean concentration k in the x-y plane at $z/H = 0.5$: (top) standard k-ε turbulences and (bottom) RNG k-ε turbulences.

means that most pollutants emitted were transported downwind before being transported upward. Concentration in the downwind direction was very low due to decreasing momentum flux.

4. Conclusions

Both the standard and the RNG κ-ε turbulence models have been applied in simulations of the flow and pollutant dispersion emitted from the ground source level in the near-wake region in the high-rise building. The results of the present study showed good agreement between the results of numerical simulations and the wind tunnel experiment for both wind flow and concentration diffusion. A rapid increment of the mean velocity with height in the near wake region was observed. The characteristics of the horizontal and vertical distributions of the mean velocity obtained by the RNG κ-ε model were similar to those obtained by the standard κ-ε model. The peak value of turbulence intensity for the numerical data and the experimental data was found near the top of the building due to the large velocity gradient. A high value of the turbulent kinetic energy was observed near the top of the building because of the strong vertical shear of the streamwise velocity there. Flow attachments were observed more quickly from the RNG κ-ε model than those from the κ-ε model. A reverse flow in the near wake region was observed. The path lines show the recirculation zone in the near wake region very clearly. A symmetric double-vortex circulation appeared. The velocity field obtained from the κ-ε turbulence models shows a vortex rotating in the upper part of the wake region. High levels of concentration diffusion occur downwind of the source, which gradually reduces as the plume moves up behind the building. The diffusion concentration was very high near the source location. The area of minimum concentration is shifted downwind of the source. The concentration results with the standard κ-ε model were in agreement with the wind tunnel results. The diffusion concentration was observed to have large gradients near the pollutant source. The area of maximum concentration is widespread, occupying the width of the building.

REFERENCES

Baik, J., J. Kim., and J. S. Fernando, 2003: A CFD model for simulating flow and dispersion. *J. Appl. Meteor.*, **42**, 1636–1648.

Counihan, J., 1969: An improved of simulating an atmospheric boundary layer in a wind tunnel. *Atmos. Environ.*, **3**, 197–214.

Dawson, P., D. E. Stock, and B. Lamb, 1991: The numerical simulation of airflow and dispersion in three-dimensional atmospheric recirculation zones. *J. Appl. Meteor.*, **30**, 1005–1024.

Fackrell, J. E., 1984: Parameters characterizing dispersion in the near wake of buildings. *Journal of Wind Engineering and Industrial Aerodynamics*, **16**, 281–291.

Flowe, A. C., and A. Kumar, 2000: Analysis of velocity fields and dispersive cavity parameters as a function of building width to building height ratio using a 3-D computer model for square buildings. *Journal of Wind Engineering and Industrial Aerodynamics*, **86**, 87–122.

Fluent Inc., 2005: FLUENT 6.2.16 user Manual, 464pp.

Franke, J., 2006: Recommendations of the cost action C14 on the use of CFD in predicting pedestrian wind environment. *Proceedings of the Fourth International Symposium on Computational Wind Engineering* (CWE2006), Yokohama, Japan, 529–532.

Halitsky, J., 1963: Gas diffusion near buildings. *ASHRAE Trans.*, **6**9, 464–485.

Hosker, R. P., Jr., 1984: Flow and diffusion near obstacles. *Atmospheric Science and Power Production*, DOE/TIC-27601, 326pp.

Higson, H. L., R. F. Griffiths, C. D. Jones, and D. J. Hall, 1994: Concentration measurement around an isolated building: A comparison between wind tunnel and field data. *Atmos. Environ.*, **28**, 1827–1936.

Hinds, W. T., 1969: Peak-to-mean concentration ratios from ground-level sources in building wakes. *Atmos. Environ.*, **3**, 145–156.

Huber, A. H., 1989: Video Images of smoke dispersion in the near wake of a model building. Part II. Cross-stream dispersion. *Journal of Wind Engineering and Industrial Aerodynamics*, **32**, 263–284.

Hunt, A., and I. P. Castro, 1984: Scalar dispersion in model building wakes. *Journal of Wind Engineering and Industrial Aerodynamics*, **17**, 89–115.

Hunt, J. C. R., W. H. Snyder, and R. E. Jr. Lawson, 1978: Flow structure and turbulent diffusion around a three-dimensional hill. Fluid Modeling Study on Effects of Stratification, Part I. Flow Structure. Report EPA-600/4-78-041, US Environmental Protection Agency, NTIS, 290pp.

Isaacson, M. S., and G. V. H. Sandri, 1990: Laboratory study of pollutant detention times in wake cavities downwind of low-rise buildings. *Journal of Wind Engineering and Industrial Aerodynamics*, **36**, 653–663.

Kim, J., and J. Baik, 2004: A numerical study of effects of ambient wind on flow and dispersion in urban street canyons using the RNG κ-ε turbulence model. *Atmos. Environ.*, **38**, 3039–3048.

Launder, B. E., and D. E. Spalding, 1974: The numerical computation of turbulent flows. *Computer Methods in Applied Mechanics and Engineering*, **3**, 269–289.

Li, W. W., and R. N. Meroney, 1983a: Gas dispersion near a cubical model building. Part I. Mean concentration measurements. *Journal of Wind Engineering and Industrial Aerodynamics*, **12**, 115–133.

Li, W. W., and R. N. Meroney, 1983b: Gas dispersion near

a cubical model building. Part II. Concentration fluctuation measurements. *Journal of Wind Engineering and Industrial Aerodynamics*, **12**, 135–147.

Li, Y., and T. Stathopoulos, 1997: Numerical evaluation of wind-induced dispersion of pollutants around a building. *Journal of Wind Engineering and Industrial Aerodynamics*, **67–68**, 757–766.

Li, Y., and T. Stathopoulos, 1998: Computational evaluation of pollutant dispersion around buildings: Estimation of numerical errors. *Journal of Wind Engineering and Industrial Aerodynamics*, **77–78**, 619–630.

Macdonald, R. W., R. F. Griffiths, and D. J. Hall, 1998: A comparison of results from scaled field and wind tunnel modeling of dispersion in arrays of obstacles. *Atmos. Environ.*, **32**, 3845–3862.

Mavroidis, I., and R. F. Griffiths, 2001: Local characteristics of atmospheric dispersion within building arrays. *Atmos. Environ.*, **35**, 2941–2954.

Mfula, A. M., V. Kukadia, R. F. Griffiths, and D. J. Hall, 2005: Wind tunnel modeling of urban building exposure to outdoor pollution. *Atmos. Environ.*, **39**, 2737–2745.

Oke, T. R., 1987: *Boundary Layer Climates*. 2nd ed., Methuen, London, UK, 474pp.

Olvera, H. A., A. R. Choudhuri, and W. Li, 2008: Effects of plume buoyancy and momentum on the near-wake flow structure and dispersion behind an idealized building. *Journal of Wind Engineering and Industrial Aerodynamics*, **96**(2), 209–228.

Patanker, S. V., 1980: *Numerical Heat Transfer and Fluid Flow*. McGraw-Hill, New York, NY, USA, 197pp.

Peterka, J. A., R. N. Meroney, and K. M. Kothari, 1985: Wind flow patterns about buildings. *Journal of Wind Engineering and Industrial Aerodynamics*, **96**, 209–228.

Robins, A. G., and I. P. Castro, 1977: A wind tunnel investigation of plume dispersion in the vicinity of a surface mounted cube. *Atmos. Environ.*, **11**, 299–311.

Saathoff, P. J., T. Stathopoulos, and M. Dobrescu, 1995: Effects of model scale in estimating pollutant dispersion near buildings. *Journal of Wind Engineering and Industrial Aerodynamics*, **54–55**, 549–559.

Sada, K., and A. Sato, 2002. Numerical calculation of flow and stack-gas concentration fluctuation around a cubical building. *Atmos. Environ.*, **36**, 5527–5534.

Snyder, W. H., 1994: Some observations of the influence of stratification on diffusion in building wakes. *Stably Stratified Flows: Flow and Dispersion over Topography*, I. P. Castro, and N. J. Rockliff, Eds., 301–324.

Wilson, D. J., and R. E. Britter, 1982: Estimates of building surface concentration from nearby point sources. *Atmos. Environ.*, **16**, 2631–2646.

Yakhot, V., S. A. Orszag, S. Thangam, T. B. Gatski, and C. G. Speziale, 1992: Development of turbulence models for shear flows by a double expansion technique. *Physics of Fluids* (*A*), **4**(7), 1510–1520.

Yassin, M. F., M. Ohba, and H. Tanaka, 2008: Experimental study on gaseous diffusion in the wake behind an isolated building. *Environment Monitoring and Assessment*, **147**(1–3), 149–158.

Zhang, Y. Q., and S. P. S. Arya, A. H. Huber, and W. H. Snyder, 1992: Simulation the effects of upstream turbulence on dispersion around a building. Report No. EPA/600/A-92/228, US Environment Protection Agency, Research Triangle Park, NC.